Journal of
Ceramic Science
and Technology

J. Ceram. Sci. Tech., 07 [04] 379-386 (2016)
DOI: 10.4416/JCST2016-00050
available online at: http://www.ceramic-science.com
© 2016 Göller Verlag

Ablation-Resistant Composite Coating of HfC-TaC-SiC for C/C Composites Deposited by Supersonic Atmospheric Plasma Spraying

Y. Yang, K. Li*, G. Liu, Z. Zhao

State Key Laboratory of Solidification Processing, Northwestern Polytechnical University, Carbon/Carbon Composites Research Center, Northwestern Polytechnical University, Xi'an 710072, China

received August 4, 2016; received in revised form August 31, 2016; accepted September 19, 2016

Abstract

HfC-TaC-SiC multiphase coating was prepared on the surface of SiC-coated carbon/carbon composites by means of supersonic atmospheric plasma spraying. The morphology and microstructure of the HfC-TaC-SiC coating were characterized with XRD and SEM. The ablation resistance test was performed with an oxyacetylene torch. The results show that the surface of the coating is dense and rough. No crack can be found. The HfC-TaC-SiC coating could protect the substrate from ablation by the generated oxide compound layer. During ablation, the new compound $Hf_6Ta_2O_{17}$ was generated, which had a single phase and high melting point. In addition, the formed Ta_2O_5 could prevent the phase transition of HfO_2 during the cooling process, which would restrict the volume expansion of HfO_2.

Keywords: Carbon/carbon composites, supersonic atmospheric plasma spraying, multiphase coating, ablation resistance

I. Introduction

Carbon/carbon (C/C) composites are considered one of the most attractive structural materials owing to their excellent physical and chemical properties [1, 2]. However, the poor oxidation resistance in the high-temperature oxidation environment of C/C composites restricts their applications [3]. Coating is an effective method to protect C/C composites from oxidation in a high-temperature oxidation environment [4, 5]. Many coating techniques, such as chemical vapor deposition, pack cementation, hydrothermal electrophoretic deposition, slurry method and plasma spraying, have achieved good effects [6–9]. Among the various techniques, supersonic atmospheric plasma spraying is a novel method with a high plasma temperature of 10 000 K and high jet velocity of 600 m/s [10, 11], which can be used to efficiently prepare an oxidation protective coating.

Refractory carbides and borides (HfC, ZrC, ZrB_2, etc.) are effective coating materials for C/C composites in a high-temperature oxidation environment [12–18]. HfC is characterized by a high melting point, high temperature stability, high hardness, and good resistance to ablation [19]. These properties make HfC an efficient coating material for protection against oxidation and ablation. However, the phase transition of the oxidation product HfO_2 may bring about cracks and break the structure of the coating. It is necessary to restrict the phase transition of HfO_2. The introduction of SiC is helpful to limit the phase transition of HfO_2 by forming a new phase of $HfSiO_4$ [20]. In addition, Ta_2O_5 has been used to inhibit the phase transition of ZrO_2, while HfO_2 has similar properties to ZrO_2. The addition of Ta_2O_5 may be useful to restrict the phase transition of HfO_2. In addition, HfO_2 could form a solid solution with Ta_2O_5, which could accelerate the sintering process and generate a dense layer during ablation [21].

In this work, we prepared a HfC-TaC-SiC multiphase coating on SiC-coated C/C composites by means of SAPS. The influence of TaC in the ablation resistance and morphology evolution of the coating were discussed. The effect of Ta_2O_5 on the sintering process was studied.

II. Experimental

(1) Preparation of HfC-TaC-SiC coating for SiC-coated C/C composites

3-D C/C composites were used as substrates with the density of 1.7 g/cm^3. Specimens were cut from the C/C composites with the size of ∅ 30 mm × 10 mm. All the specimens were hand-abraded and cleaned.

A SiC bonding layer was prepared on the surface of C/C composites by means of pack cementation. The precursor powders consisted of 75 wt% Si, 15 wt% C, and 10 wt% Al_2O_3. The specimens were embedded in the precursor powders, and then heated to 2173 – 2373 K and preserved for 2 h in an argon-protective atmosphere. The detailed preparation process has been reported [22]. Fig. 1 shows the XRD patterns and surface morphology of the inner SiC coating, which is composed of lamellar SiC and liquated Si.

The HfC-TaC-SiC (HTS) multiphase coating was deposited on the surface of the SiC-coated C/C composites by means of SAPS in air. Before the spraying process, the mixture of HfC, TaC and SiC particles was pelleted in a spray dryer to ensure the liquidity of the particles. The molar ratio is 2: 2: 1. During the spraying process, the samples

* Corresponding author: likezhi@nwpu.edu.cn

were held in an assembly fixture and positioned perpendicular to the plasma torch. The technological parameters of the whole preparation process are listed in the Table 1.

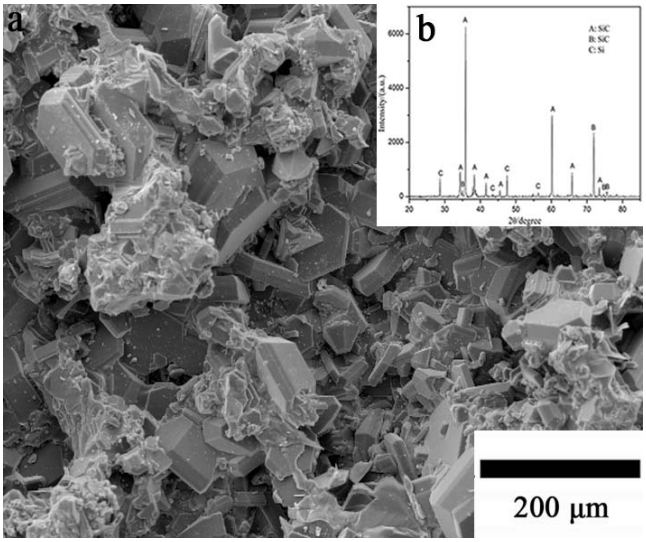

Fig. 1: XRD patterns and surface SEM image of the inner SiC coating.

Table 1: Details of the spraying parameters for the HfC-SiC coating.

Content		Parameters
Spraying current	(A)	400
Spraying voltage	(V)	120
Primary gas Ar	(L/min)	75
Carrier gas Ar	(L/min)	10
Second gas H_2	(L/min)	5
Powder feed rate	(g/min)	30
Spraying distance	(mm)	100
Nozzle diameter	(mm)	5.5

(2) Ablation test and microstructure analysis

The ablation test on the coated samples was performed with an oxyacetylene torch. The pressure of O_2 and C_2H_2 were 0.4 MPa and 0.095 MPa, while their fluxes were 0.244 L/s and 0.167 L/s, respectively. The heat flux of the oxyacetylene torch was 2.38 MW/m^2. The distance between the nozzle tip of the oxyacetylene gun and the coated surface was 10 mm. The inner diameter of the oxyacetylene gun tip was 2 mm. The surface temperature of the samples was estimated to be 2200 ± 100 K measured with an infrared thermometer (Raytek MR1SCSF). The ablation angle was 90°.

The mass ablation rate of the sample was obtained based on the mass change before and after ablation. The ablation rate of the sample was the average ablation rate of three samples.

The crystalline structure and morphology of the as-obtained coatings and ablated coatings were investigated by means of x-ray diffraction (XRD, X'Pert Pro, PANalytical, Almelo, the Netherlands), scanning electron microscopy (SEM, JSM6460, JEOL Ltd., Mitaka, Japan) along with energy-dispersive spectroscopy (EDS, Oxford INCA).

III. Results and Discussion

(1) Microstructure and morphology of the HTS coating

The XRD patterns of the HTS before and after spraying are shown in Fig. 2. It can be seen that the detected diffraction peaks are in accordance with the JCPDS card No. 03–065–0964, No. 03–065–8794 and No. 00–040–1173. However, the carbides were partly oxidized after spraying, which resulted from the reactions between the carbides and oxygen during the spraying and cooling process in air.

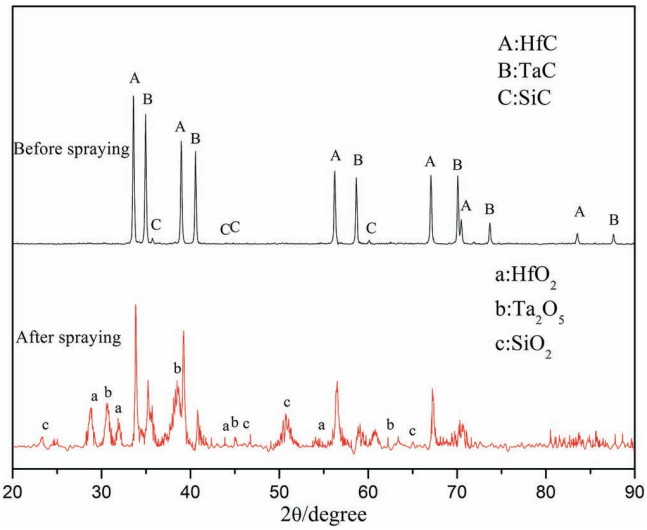

Fig. 2: XRD patterns of the HTS before and after spraying.

The surface and cross-section morphology of the HTS coating are shown in Fig. 3. From the Fig. 3a, it can be seen that the surface is rough and dense, and no crack can be found on the surface. However, from the high magnification SEM image (Fig. 3b), it can be seen that some pinholes are distributed non-uniformly on the surface, which resulted from the evaporation of oxidation products. From Fig. 3c, it can be observed that the thickness of the outer HTS coating is about 200 μm. The structure is dense without cracks. The boundary between the HTS coating and the SiC inner coating, that is the mechanical bond between the two coatings, is distinct. In addition, according to the elements line analysis, as shown in Fig. 3d, the O element is mainly distributed in the range of 0–200 μm, which means that the carbides were oxidized during the whole spraying process.

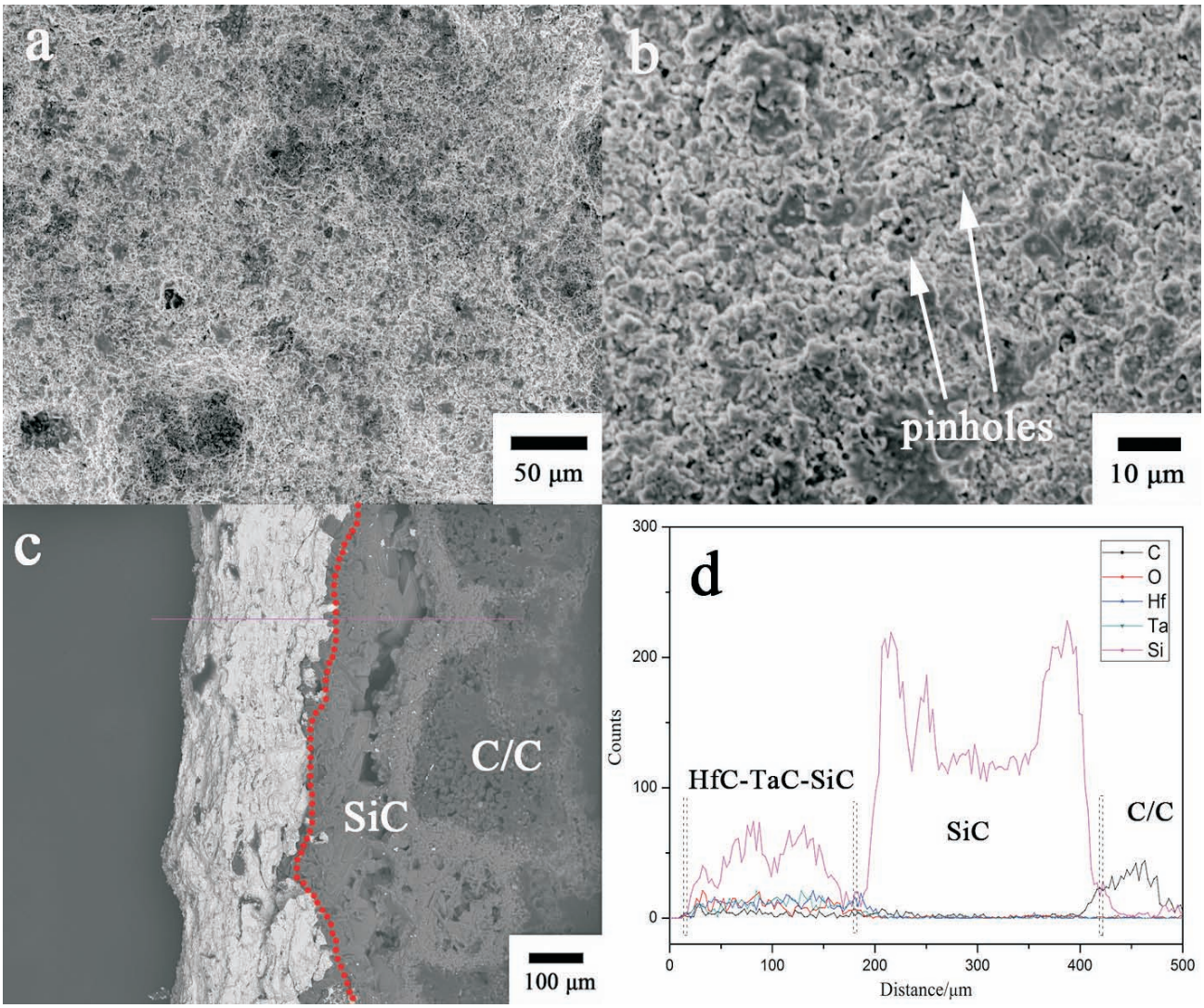

Fig. 3 : Surface (a), (b) and cross-section (c) morphology and elements line analysis (d) of the HTS coating.

(2) Ablation properties

An oxyacetylene torch was used to test the ablation properties of the HTS coating. The coated samples were exposed to the flame for 30 s, 60 s, 90 s and 120 s, respectively. Fig. 4 shows the surface temperature variation of the HTS samples during ablation. It can be seen that the surface temperature rose rapidly in the initial stage and kept at about 2200 K after ablation for 50 s. In the first 50 s, the carbides were oxidized and released heat, which resulted in the rapid increase of the surface temperature. The mass ablation rates of the HTS samples are -0.543 mg/s, 0.022 mg/s, 0.433 mg/s, 0.741 mg/s, respectively, which meant the weight of the HTS coating increased first and then decreased during ablation. The increase in weight mainly resulted from the oxidization of carbides, while the decrease was due to the evaporation of low-melting-point oxides such as Ta_2O_5 and SiO_2.

During ablation, the samples were exposed in an oxygen-rich environment [23] and some severe reactions took place in the ablation center region of the coating. When the surface temperature stayed at 2200 K, the following reactions may take place:

$$2HfC\ (s) + 3O_2\ (g) \rightarrow 2HfO_2\ (s) + 2CO\ (g) \quad (1)$$

$$4TaC\ (s) + 7O_2\ (g) \rightarrow 2Ta_2O_5\ (s) + 4CO\ (g) \quad (2)$$

$$2SiC\ (s) + 3O_2\ (g) \rightarrow 2SiO_2\ (l) + 2CO\ (g) \quad (3)$$

$$Ta_2O_5\ (s) \rightarrow Ta_2O_5\ (l) \quad (4)$$

$$6HfO_2\ (s) + Ta_2O_5\ (s) \rightarrow Hf_6Ta_2O_{17}\ (s) \quad (5)$$

$$SiO_2\ (s) \rightarrow SiO_2\ (l) \quad (6)$$

$$HfO_2\ (s) + SiO_2\ (s) \rightarrow HfSiO_4\ (s) \quad (7)$$

Fig. 5 shows the XRD patterns of the HTS coatings after ablation for different times. In the first 30 s, the surface temperature was relatively low, and the main reactions were the oxidation of carbides. As shown in the XRD patterns, the diffraction peaks of different oxides such as Ta_2O_5, HfO_2, and SiO_2 were detected after ablation for 30 s. Meanwhile, the newly formed HfO_2 could react with Ta_2O_5 to generate new stable phases $Hf_6Ta_2O_{17}$ [24]. In addition, during the cooling process, HfO_2 could react with SiO_2 and form another phase $HfSiO_4$ [25]. As the ab-

lation went on, the surface temperature of the coating rose to about 2200 K, exceeding the melting point of Ta_2O_5 (2058 K) and SiO_2 (1873 – 1973 K) [26], which resulted in the evaporation and weight loss. The XRD patterns indicate that the diffraction peak intensity of Ta_2O_5 and SiO_2 decreased. Meanwhile, the further generated $HfSiO_4$ was also reduced owing to the reduction of SiO_2. However, the solid solution sintering of the oxides also played an important role during ablation. The high temperature was beneficial for sintering to form the stable $Hf_6Ta_2O_{17}$, which resulted in the increase of the diffraction peaks' intensity. In addition, the high-pressure environment caused by the oxyacetylene flame was also helpful to accelerate the sintering process. During ablation, the Ta_2O_5 evaporated and the oxides were sintered simultaneously. When the samples were ablated for 120 s, the Ta_2O_5 and SiO_2 in the external coating were almost consumed, leaving the $Hf_6Ta_2O_{17}$ and HfO_2.

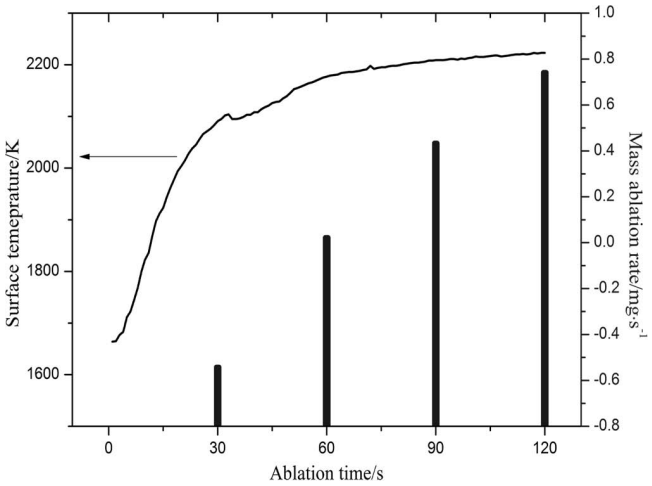

Fig. 4: Surface temperature and mass ablation rate of the HTS samples.

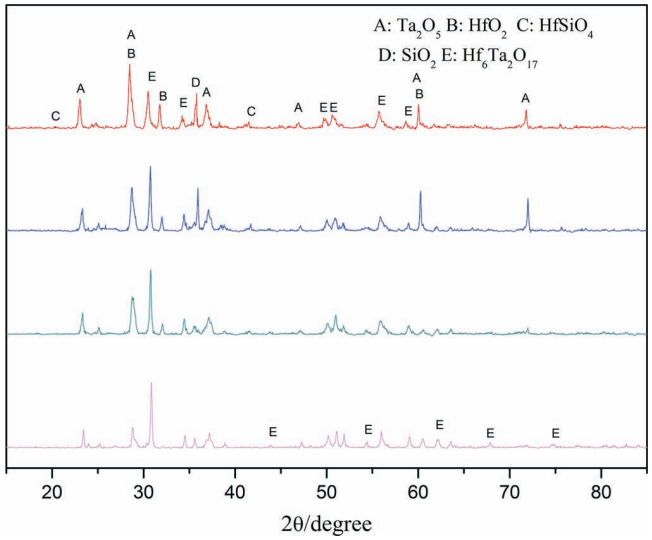

Fig. 5: XRD patterns of the HTS coatings after ablation for different times.

(3) Ablation morphology

Fig. 6 shows the surface morphology and EDS analysis of HTS coatings in the ablation center region after ablation for different times. In the first 30 s, the temperature was relative low and the main reactions were the oxidation of carbides. As shown in Fig. 6a, the initial rough surface was translated to small stacked oxide grains with a dense structure. Some pinholes were distributed on the surface, which may result from the volatilization of generated gases. According to the EDS analysis of spot A (shown in Fig. 6e), it can be seen that the surface consisted of Hf, Ta, Si and O elements, which meant the carbides had been oxidized completely. In addition, the ratio of Hf, Ta and Si had changed compared to the initial ratio (2: 2: 1), which resulted from the evaporation of generated Ta_2O_5 and SiO_2. As the ablation went on, more oxides were generated on the surface of the coating, which resulted in a denser structure and reduction of pinholes (Fig. 6b). As shown in Fig. 6c, with the increase in the ablation time to 90 s, the surface temperature remained at about 2200 K, which could lead to the evaporation of generated Ta_2O_5 and SiO_2 and the formation of pores. In addition, the solid solution sintering in the high temperature brought about the volume shrinkage of the conglomerated grains, thus leading to the loose structure. After ablation for 120 s, as shown in Fig. 6d, the evaporation and solid solution sintering were accelerated, which made the pores on the surface more obvious. As shown in Fig. 6f, according to the EDS analysis of spot B, the intensity of the Ta peak clearly decreased. Meanwhile, on the basis of the elements ratio, it indicated that all of the Si and half of the Ta had evaporated. To summarize, the oxidation of carbides played a major role at the temperature-rise stage, while the sintering and evaporation of formed oxides played the important roles during the rest of the ablation process.

The cross-section micrographs of the HTS coatings after ablation for different times are shown in Fig. 7. It can be seen that the depth of the oxidation region increased with the increase in ablation time, which resulted from the gradual permeation of the oxygen. In addition, the thickness of the coating was reduced owing to the evaporation of generated Ta_2O_5 and SiO_2. According to the EDS analysis, the content of Ta and Si elements in the external coating decreased from Fig. 7a to Fig. 7d, which indicated the evaporation of Ta_2O_5 and SiO_2. As shown in Fig. 7a, a fine crack appeared in the cross-section after ablation for 30 s, which resulted from the mismatch of the coefficient of thermal expansion between the oxidized external coating and the unreacted coating. During ablation, the formed HfO_2 was tetragonal-HfO_2, and translated to monoclinic-HfO_2 after cooling, which would lead to crack expansion [21]. However, Ta_2O_5 could restrict the phase transition of HfO_2 based on the solution effect [27]. In addition, the further formed $HfSiO_4$ can not only consume the HfO_2 but have a pinning effect to prevent extension of the cracks [28]. With the increase of ablation time, the reduction of Ta_2O_5 would lead to the increase of m-HfO_2, which was translated from t-HfO_2 after cooling. Meanwhile, the further formed $HfSiO_4$ also decreased owing to the decrease in SiO_2. The phase transition of HfO_2 brought about volume expansion, which resulted in crack propagation and structural failure.

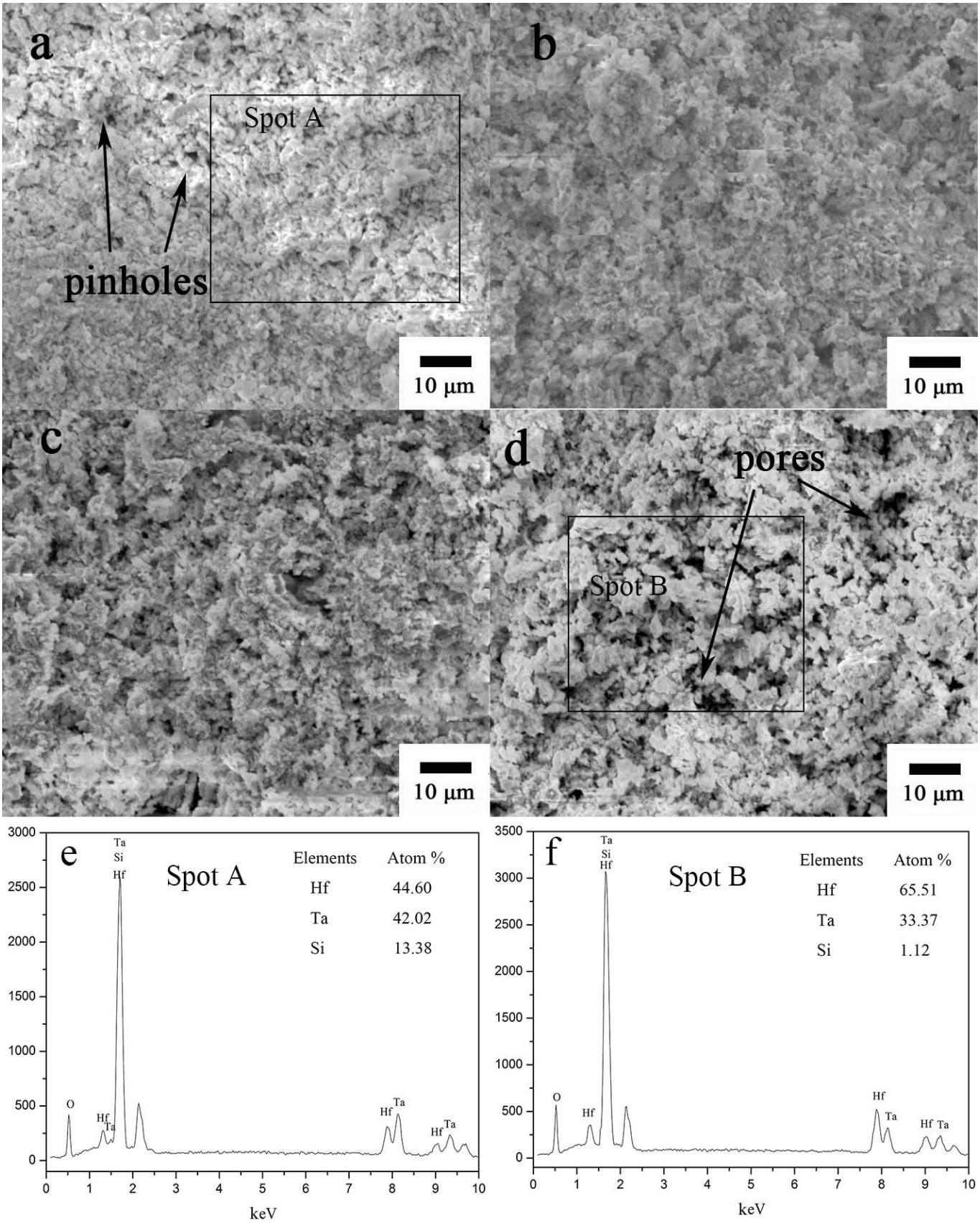

Fig. 6 : Surface morphology and EDS analysis of HTS coatings in the ablation center region after ablation for different times: (a) 30 s; (b) 60 s; (c) 90 s; (d) 120 s; (e) EDS of spot A; (f) EDS of spot B.

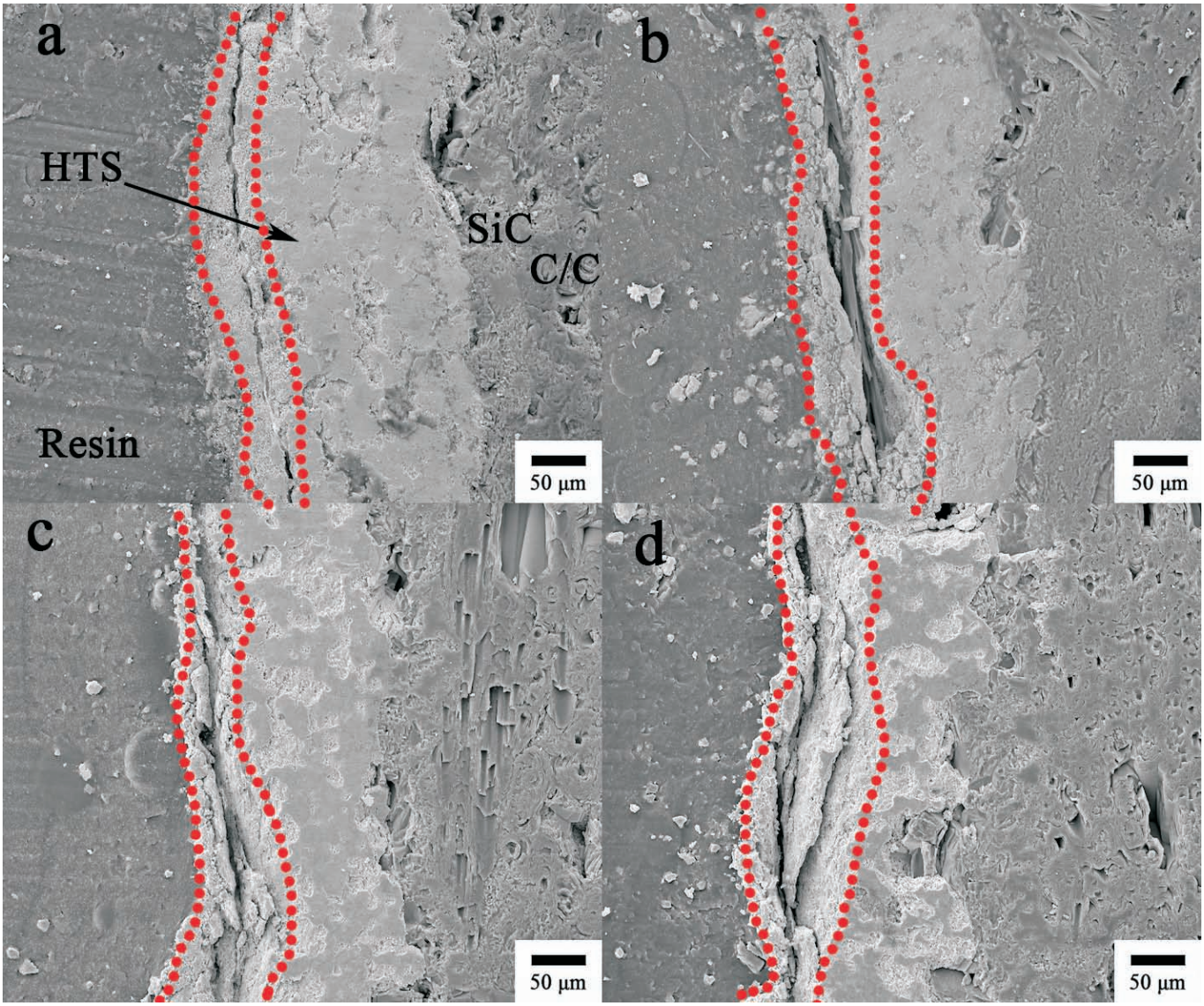

Fig. 7 : Cross-section micrographs of HTS coatings in the ablation center region after ablation for different times: (a) 30 s; (b) 60 s; (c) 90 s; (d) 120 s.

IV. Conclusions

The deposited HfC-TaC-SiC multiphase coating was mainly composed of different carbides and their oxides, which were oxidized during the spraying process. After ablation for different times, the weight of the HTS samples first increased and then decreased. During ablation, the oxidation of carbides was in the important position at the temperature-rise stage, while the sintering and evaporation of the newly formed oxides played a major role during the remaining ablation process. The evaporation of Ta_2O_5 and SiO_2 resulted in the formation of pores and a loose structure. In addition, the stable phase $Hf_6Ta_2O_{17}$ was generated by the solid solution sintering in the ablation. The phase transition of HfO_2 could be inhibited by the generated Ta_2O_5 during the short ablation time. $HfSiO_4$ can have a pinning effect to prevent crack extension. However, with the increase of ablation time and the evaporation of Ta_2O_5 and SiO_2, the volume expansion of HfO_2 would lead to obvious cracks. Ta_2O_5 acted as a sintering aid during ablation. The sintering process could be accelerated with the introduction of sintering aid in the HfC coating, which was beneficial for the formation of a stable phase $Hf_6Ta_2O_{17}$ with a high melting point.

Acknowledgments

This work was supported by the National Natural Science Foundation of China under Grant No. 50902111 and 5120209, and supported by the "111" project under grant No. 08040 and the Research Fund of the State Key Laboratory of Solidification Processing (NWPU), China (Grant No. 142-TZ-2016).

References

1 Li, L., Li, H., Yin, X., Chu, Y., Chen, X., Fu, Q.: Oxidation protection and behavior of *in-situ* zirconium diboride-silicon carbide coating for carbon/carbon composites, *J. Alloy. Compd.*, **645**, 164 – 170, (2015).

2 Zhang, J.P., Fu, Q.G., Zhuang, L., Chen, X., Li, H.J., Nan, X.Y., Sun, C., Xie, J.: Oxidation behaviour of SiC coated C/C-ZrC-ZrB_2-SiC composites in wind tunnel at 1600 °C, *Surf. Eng.*, **31**, 368 – 372, (2015).

3 Zhuang, L., Fu, Q.-G., Zhang, J.-P., Guo, Y.-A., Li, H.-J., Shan, Y.-C.: Effect of pre-oxidation treatment on the bonding

strength and thermal shock resistance of SiC coating for C/C-ZrC-SiC composites, *Ceram. Int,*, **41**, 6956 – 6964, (2015).

4 ZhongLiu, W., Peng, X., Zhuan, L., Wen, H., Heng, L., XiaoYu, Y., Yang, L., WenBo, C.: Microstructure and oxidation behavior of sol-gel mullite coating on SiC-coated carbon/carbon composites, *J. Eur. Ceram. Soc.*, **35**, 3789 – 3796, (2015).

5 Chu, Y., Li, H., Luo, H., Li, L., Qi, L.: Oxidation protection of carbon/carbon composites by a novel SiC nanoribbon-reinforced SiC-Si ceramic coating, *Corros. Sci.*, **92**, 272 – 279, (2015).

6 Liu, J., Cao, L.-Y., Huang, J.-F., Xin, Y., Yang, W.-D., Fei, J., Yao, C.-Y.: A $ZrSiO_4$/SiC oxidation protective coating for carbon/carbon composites, *Surf. Coat. Tech.*, **206**, 3270 – 3274, (2012).

7 Wang, S.-L., Li, K.-Z., Li, H.-J., Zhang, Y.-L., Zhang, W.-Y.: Ablation behavior of CVD-ZrC coating under oxyacetylene torch environment with different heat fluxes, *Int. J. Refract. Met. H.*, **48**, 108 – 114, (2015).

8 Zhang, Y., Hu, Z., Li, H., Ren, J.: Ablation resistance of ZrB_2-SiC coating prepared by supersonic atmosphere plasma spraying for SiC-coated carbon/carbon composites, *Ceram. Int.*, **40**, 14749 – 14755, (2014).

9 Feng, T., Li, H.J., Fu, Q.G., Shi, X.H., Shen, X.T.: $MoSi_2$-Si-B/SiC double-layer oxidation protective coating for carbon/carbon composites, *Surf. Eng.*, **27**, 345 – 349, (2011).

10 Xing, Z., Wang, H., Zhu, L., Zhou, X., Huang, Y.: Properties of the $BaTiO_3$ coating prepared by supersonic plasma spraying, *J. Alloy. Compd.*, **582**, 246 – 252, (2014).

11 Sun, J., Fu, Q.-G., Liu, G.-N., Li, H.-J., Shu, Y.-C., Fan, G.: Thermal shock resistance of thermal barrier coatings for nickel-based superalloy by supersonic plasma spraying, *Ceram. Int.*, **41**, 9972 – 9979, (2015).

12 Yang, Y., Li, K., Li, H.: Ablation behavior of HfC coating prepared by supersonic plasma spraing for SiC-coated C/C composites, *Adv. Compos. Lett.*, **24**, 107 – 112, (2015).

13 Yao, X., Li, H., Zhang, Y., Li, K., Fu, Q., Peng, H.: Ablation behavior of ZrB_2-based coating prepared by supersonic plasma spraying for SiC-coated C/C composites under oxyacetylene torch, *J. Therm Spray Techn.*, **22**, 531 – 537, (2013).

14 Hu, M.H., Li, K.Z., Li, H.J., Wang, B., Ma, H.L.: Double layer $ZrSi_2$-ZrC-SiC/SiC oxidation protective coating for carbon/carbon composites, *Surf. Eng.*, **31**, 335 – 341, (2014).

15 Ren, X., Li, H., Fu, Q., Li, K.: Ultra-high temperature ceramic TaB_2-TaC-SiC coating for oxidation protection of SiC-coated carbon/carbon composites, *Ceram. Int.*, **40**, 9419 – 9425, (2014).

16 Ren, X., Li, H., Fu, Q., Li, K.: $Ta_xHf_{1-x}B_2$-SiC multiphase oxidation protective coating for SiC-coated carbon/carbon composites, *Corros. Sci.*, **87,** 479 – 488, (2014).

17 Wu, Z.T., Qi, Z.B., Zhang, D.F., Wang, Z.C.: Microstructure, mechanical properties and oxidation resistance of (Zr, Hf)N_x coatings by magnetron co-sputtering, *Surf. Coat. Tech.*, **276**, 219 – 227, (2015).

18 Chicardi, E., Córdoba, J.M., Gotor, F.J.: High temperature oxidation resistance of (Ti,Ta)(C,N)-based cermets, *Corros. Sci.*, **102**, 125 – 136, (2016).

19 Wang, Y.-L., Xiong, X., Li, G.-D., Liu, H.-F., Chen, Z.-K., Sun, W., Zhao, X.-J.: Ablation behavior of HfC protective coatings for carbon/carbon composites in an oxyacetylene combustion flame, *Corros. Sci.*, **65**, 549 – 555, (2012).

20 Yang, Y., Li, K., Zhao, Z., Li, H.: Ablation resistance of HfC-SiC coating prepared by supersonic atmospheric plasma spraying for SiC-coated C/C composites, *Ceram. Int.*, **42**, 4768 – 4774, (2015).

21 Fu, Q.G., Li, H.J., Shi, X.H., Li, K.Z., Sun, G.D.: Silicon carbide coating to protect carbon/carbon composites against oxidation, *Scripta Mater.*, **52**, 923 – 927, (2005).

22 Liu, L., Li, H., Feng, W., Shi, X., Li, K., Guo, L.: Ablation in different heat fluxes of C/C composites modified by ZrB_2-ZrC and ZrB_2-ZrC-SiC particles, *Corros. Sci.*, **74**, 159 – 167, (2013).

23 Li, M., Xu, Q., Wang, L.: Thermal conductivity of $(Hf_{1-x}Zr_x)_6Ta_2O17$ (x = 0, 0.1, 0.3 and 0.5) ceramics, *Ceram. Int.*, **38**, 4357 – 4361, (2012).

24 Bundschuh, K., Schütze, M.: Materials for temperatures above 1500 °C in oxidizing atmospheres. part I: basic considerations on materials selection, *Mater. Corros.*, **52**, 204 – 212, (2001).

25 Dean, J.A.: Lange's Handbook of Chemistry, McGraw-Hill, 1999.

26 Dean, J.A.: Lange's Handbook of Chemistry, McGraw-Hill, 1999.

27 Samaranch, B., Clet, G., Houalla, M., Gélin, P., Homs, N.: Synthesis and characterization of Ta_2O_5-ZrO_2 Systems: Structure, surface acidity, and catalytic properties, *Chem. Mater.*, **19**, 1445 – 1451, (2007).

28 Ren, X., Li, H., Chu, Y., Fu, Q., Li, K.: Ultra-High-temperature ceramic HfB_2-SiC coating for oxidation protection of SiC-coated carbon/carbon composites, *Int. J. Appl. Ceram. Tech*, **12**, 560 – 567, (2015).